

# Additive Manufacturing of Embedded Passive Electronic Components

Ariful Islam, Md Shahriar Forhad, Jianzhi Li, and Farid Ahmed

Institute of Advanced Manufacturing, The University of Texas Rio Grande Valley, TX 78529

## Abstract

Additive Manufacturing of Electronics is transforming the production of electronic devices by allowing customized designs with complex three-dimensional geometries and flexible structures. Traditional printed circuit board (PCB) based fabrication often struggles with rigid layouts, parasitic losses, and oxidation of exposed traces. These limitations signify why embedded additive approaches are becoming increasingly important. In this study, we demonstrated 3D printing of various passive electronic components, including resistors (R) and capacitors (C). They were fully embedded inside the insulating materials. We simultaneously deposited conductive material (silver ink) and dielectric material (acrylic ink) on the substrates used in this work to fabricate embedded circuits with complex geometry. 3D printing of embedded resistors and capacitors was demonstrated to analyze the performance of electronic filters. We have studied the electrical properties of these components by studying their resistance, capacitance, and charging and discharging behaviors based on the components' geometric configurations. We investigated how structural parameters influence the performance of 3D-printed passive components and explored the process's potential for manufacturing various embedded electronics with customizable features.

In this study, we successfully printed resistors with values ranging from less than  $1\ \Omega$  up to about  $32\ \Omega$ , as well as multilayer capacitors with capacitances approaching  $3\ \text{nF}$ . These results are well-suited for compact filter applications operating in the megahertz range. To further validate circuit-level performance, we integrated a printed resistor of  $11.63\ \Omega$  with a  $6.95\ \text{nF}$  capacitor to form a first-order RC low-pass filter. The filter exhibited a theoretical cutoff frequency of approximately  $1.97\ \text{MHz}$ , and the measured RMS and amplitude responses matched the expected  $-3\ \text{dB}$  roll-off near cutoff, confirming both the accuracy of the printed components and the reliability of the embedded design. By fully embedding these components, our approach not only protects them from environmental damage but also makes the overall design smaller and more reliable—an advantage for future applications in RF circuits, IoT devices, and aerospace systems.

## Introduction

Passive electronic components, such as inductors, capacitors, and resistors are essential for power management, signal conditioning, and energy storage in electronic systems. They enable the integration of diverse power sources and device requirements through functions such as filtering, voltage regulation, and feedback control.[1] Passive components on a flexible substrate are building blocks for organic printed electronics [2]. Conventional fabrication of passive components relies on rigid, planar circuit boards and subtractive processes (e.g., etching, machining), which restrict complex geometry and often entail multiple processing steps and material waste [3]. Additive manufacturing (AM) offers a compelling alternative by allowing

complex 3D geometries to be built up directly from digital designs, thereby simplifying supply chains and reducing waste [4] [5][6]. In other words, AM moves the process away from cutting and etching materials and instead builds electronics layer by layer, giving designers more freedom, reducing reliance on bulky rigid parts, and saving materials in the process.

For example, AM methods can print conductive and dielectric materials on flexible or curved surfaces and enable the embedding of electronic components inside structural parts. These techniques enable rapid prototyping and customization of circuits without masks or tooling [3][7]. Additive manufacturing techniques for electronics encompass a range of approaches. [6] Inkjet printing is one of the advanced non-contact and maskless additive printing methods that offers very high resolution.[7][8] Inkjet printing is widely used due to its compatibility with a variety of inks (metals, polymers, ceramics, carbon, and 2D materials) and its ability to deposit micron-scale droplets precisely [3] [8]. Despite these advances, most demonstrations remain focused on components printed on the surface, where issues such as oxidation, parasitic effects, and limited scalability still appear. This gap motivates researchers to move toward embedded printing approaches. For instance, inkjet printing has been employed to construct multilayer R–C–L networks by successively printing conductive and dielectric inks [9]. Aerosol-jet printing (AJP) is another droplet-based method that can focus nanoscale ink particles through a nozzle, enabling finer feature sizes and the ability to print on 3D-shaped substrates [3]. Direct ink writing (extrusion-based 3D printing) can dispense viscous functional inks (e.g., ceramic-filled polymers or pastes) into arbitrary 3D paths; this has been used for printing conductive traces and structures. Traditional fused-deposition modeling (FDM) 3D printing has also been adapted by utilizing dual nozzles or conductive filaments. For example, polymer scaffolds have been printed and subsequently filled with liquid metal to form inductors and capacitors [10]. Again, vat photopolymerization (stereolithography/DLP) is being applied to electronics; for example, high-resolution printing combined with metallization has produced 3D microwave filters, antennas, soft robots, and strain sensors [5][11].

Several research groups have demonstrated the use of printed resistors using various inks and methods. For example, Yadav reported the fabrication of microresistors using silver ink by the microcantilever printing method [12]. Jung et al. [2] demonstrated that inkjet-printed PEDOT: PSS resistors on flexible substrates can achieve resistances spanning five orders of magnitude by varying ink formulation and over-printing. Ostfeld et al. [1] reported screen-printed inductors, capacitors, and resistors on flexible PET substrates. The group achieved resistors with a range of  $k\Omega$  to  $M\Omega$ , with a 10% deviation. They also demonstrated a flexible RLC circuit using these passive components, thereby reducing inductor loss, which is a concern for power electronics. Conductive nanomaterials have also been exploited. Zhang et al. [4] investigated aqueous and organic  $Ti_3C_2T_x$  MXene inks for extrusion and inkjet printing on plastic and paper substrates without additives. They have printed conductive tracks, resistors, and supercapacitors. These explorations reveal that printed resistor values can be tuned by ink type. Printable capacitors have similarly been realized. Mikolajek et al. [7] fabricated fully inkjet-printed metal–insulator–metal capacitors by alternating silver electrodes and a  $Ba_{0.6}Sr_{0.4}TiO_3$ -poly(methyl methacrylate) (PMMA) composite dielectric. They were able to improve permittivity by doping ceramics into the polymer, compared to the pure polymer. The printed dielectric layers achieved  $\epsilon_r \approx 20$ –55 (at 1 kHz), depending on the ceramic loading. Multilayer capacitor designs have also been made by printing polymerizable composite inks: Reinheimer et al. [6] printed a stack of three polymer–

ceramic dielectric layers (50:50 BST–PEG diacrylate) separated by four printed Ag electrodes, yielding a 3D multilayer capacitor on PET. Screen printing has been used to deposit high-k inks as well; for example, BaTiO<sub>3</sub>-loaded inks were screen-printed as capacitor dielectrics between silver layers [1]. These additive approaches produce thicker dielectric films than lithographically defined capacitors, which pose a challenge to achieving high capacitance density and low loss.

Beyond individual elements, complete printed passive networks, such as filters, waveguides, and antennas, have been demonstrated [13][14]. Ostfeld et al. [1] demonstrated a printed RLC step-up voltage regulator by integrating their printed inductors, resistors, and capacitors on a flexible circuit. Wu et al. [10] also built a 3D printed LC tank circuit by combining a solenoid inductor with a parallel-plate capacitor. Again, photopolymer-based 3D printing (with metal plating) enabled a compact 3D low-pass filter and a directional coupler that are not possible with planar fabrication [6] [7][13]. Robles et al. [15] utilized 3D printing technology and the Fused Filament Fabrication (FFF) method to print high-frequency filters. Niu et al.[16] employed the Aerosol Jet Printing method to print conformal temperature sensors using silver nanoparticle-doped reduced oxide graphene ink. These works demonstrate that passive filter networks and resonators can be printed, albeit typically as laboratory demonstrations with lower performance compared to conventional parts.

Despite progress, key challenges remain. Printing resolutions are coarser than those achievable with semiconductor lithography or precision printed circuit board (PCB) etching, which can limit high-frequency performance [5] [17]. Printed metal traces often have lower conductivity (due to porosity or incomplete sintering) than bulk metal, resulting in increased resistive losses. Thick printed dielectrics tend to have lower permittivity and higher loss than thin-film dielectrics [18]. Ensuring good adhesion and alignment between successive printed layers can also be difficult. Researchers have been attempting to fabricate embedded resistors and capacitors for a long time using various approaches. While structure–property relationships of passive components are well understood, prior studies have primarily focused on surface-printed or conventionally assembled embedded passive components. In contrast, there is a lack of research on fully embedded, multi-material 3D-printed passive components that eliminate the need for external discrete parts. While we vary the printed 3D geometry to tune electrical values, the novelty of this work is in the embedding strategy (PCB printing method) and sustainable fabrication.

In this paper, we demonstrate a novel dual-ink 3D-printing approach to fabricate discrete multilayered and fully embedded resistors, capacitors, and low-pass filters using silver-based conductive ink and acrylic (polymer) ink, resulting in a compact, waste-free, and post-processing-free manufacturing process with no toxic chemicals involved. By embedding these passive elements directly into the insulating substrate, our approach makes the components more stable in various environments, reduces unwanted parasitic effects, and enables more compact designs—clear advantages over earlier methods that only printed components on the surface.

### **Experimental Methods**

A 3d printer shown in Figure 1, called DragonFly IV from Nano Dimension, was employed to print all samples. Initially, the passive components were designed using 3D software (SolidWorks). Then, slicer software was used to build up the layer-by-layer structure. The machine features two

print heads, each consisting of 256 nozzles. One print head is for dielectric ink and another for conductive ink. Silver nanoparticles were used as conductive ink, and an epoxy polymer (acrylic) was used as a dielectric ink. The temperature of the print head was 40 °C and 55 °C, respectively. The printing bed temperature was 160 °C. The ink comes through the nozzle and deposits on the substrate according to the print job. A kapton sheet was used as a substrate. Then, it proceeds to the curing station, where the deposited ink solidifies and the structure is built. The machine features two curing stations. A UV light is used to cure the dielectric ink, and an IR light is used to cure the conductive ink.



*Figure 1: DragonFly IV printer.*

## Results and Discussions

### **Ink properties:**

A nanoparticle-based silver conductive ink was utilized for printing our samples. This ink is formulated by the manufacturer of the DragonFly IV system, enabling the deposition of high-resolution conductive traces. Silver (Ag) is a highly conductive metal. The ink demonstrated strong adhesion to the substrate and compatibility with the surrounding dielectric polymer, maintaining good mechanical integrity during and after processing. Tables 01 and 02 present various properties of the dielectric and conductive inks, as specified by the manufacturing company (Nano-Dimensions) of our printer.

**Table 01:** Dielectric ink properties [19].

f (GHz)	0.2	1.0	2.5	5.0	7.5	10.0	30.0	40.0	50.0	65.0
Dielectric Constant (Dk)	2.96	2.89	2.85	2.83	2.81	2.80	2.83	2.82	2.82	2.81
Tangential loss (Df)	0.034	0.026	0.018	0.018	0.021	0.021	0.016	0.016	0.016	0.014

**Table 02:** Conductive ink properties [19].

	CI 90072	Unit	Test Method
Conductivity (silver nano particles) at 20 °C <sup>(1)</sup>	2.21x10 <sup>7</sup> ±0.95x10 <sup>7</sup>	S/m	Printing & sintering conditions dependent
Max reflow solder temperature <sup>(2)</sup>	165	°C	Using: Quick Chip TS391LT (138°C <sup>***</sup> )/ KOKI TB48-M742 (138°C <sup>***</sup> ) Paste.
Max manual soldering temperature <sup>(2)</sup>	220	°C	
Roughness Ra	<2µm Top and Internal	µm	
	<0.25 Bottom	µm	
(1) Bulk silver conductivity = 6.30x10 <sup>7</sup> σ (S/m) at 20 °C (2) Refer to Nano Dimension Manual Soldering Guidelines. (3) Melting temperature per vendor’s specification.			

The conductivity of the Ag nanoparticles at 20 °C is 2.21\*10<sup>7</sup>±0.95\*10<sup>7</sup> S/m. The resistivity of the ink was calculated according to the following equations:

$$\rho = \frac{1}{\sigma} \dots\dots\dots (1)$$

$$\Delta\rho = \frac{d\rho}{d\sigma} \Delta\sigma = \frac{1}{\sigma^2} \Delta\sigma \dots\dots\dots (2)$$

Where ρ represents the resistivity of the ink, measured in ohm-meters (Ω·m), σ represents the electrical conductivity, measured in siemens per meter (S/m), Δρ is the uncertainty (or margin of error) in resistivity, and Δσ is the uncertainty in conductivity.

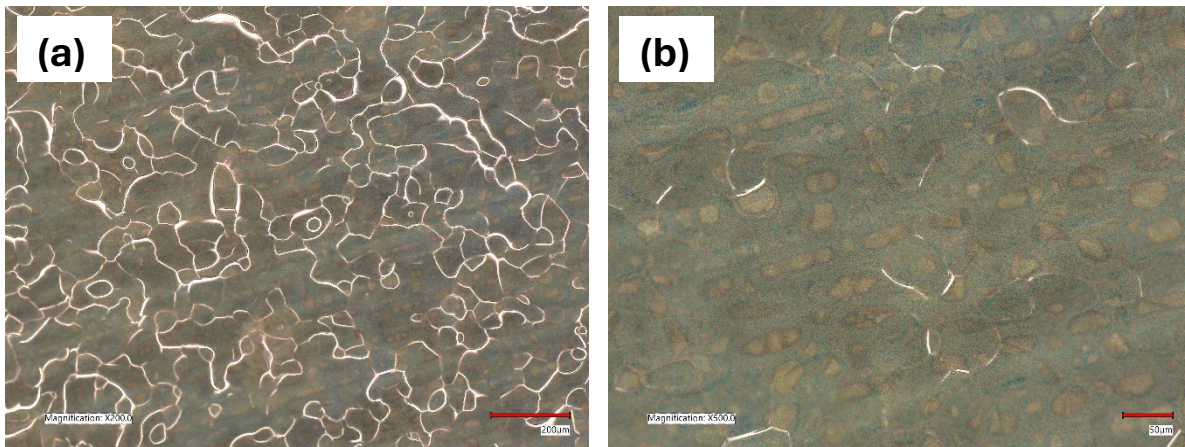


**Figure 2:** Morphology of the Ag ink after printing and curing.

Figure 2 reveals the morphology of the silver ink. An IR light station cured the ink during the printing process. The nano silver strands seem to be homogeneously dispersed in the dielectric material.

An acrylic-based dielectric polymer was used as the insulating material in the printed resistor structures. This material was selected for its excellent printability, chemical compatibility with the conductive silver ink, and stable dielectric properties. The acrylic dielectric ink was formulated for jetting using the DragonFly IV system, allowing for precise deposition alongside conductive traces without cross-contamination. Upon curing by UV light, the polymer exhibited good adhesion to the substrate and neighboring conductive features. Figure 3 shows the variation of dielectric constant and tangential loss with frequency.

These measurements were done using a SPEAG DAK\_TL 3.5-P contact probe beam on the surface at  $22 \pm 3$  °C by the nano-dimension company.

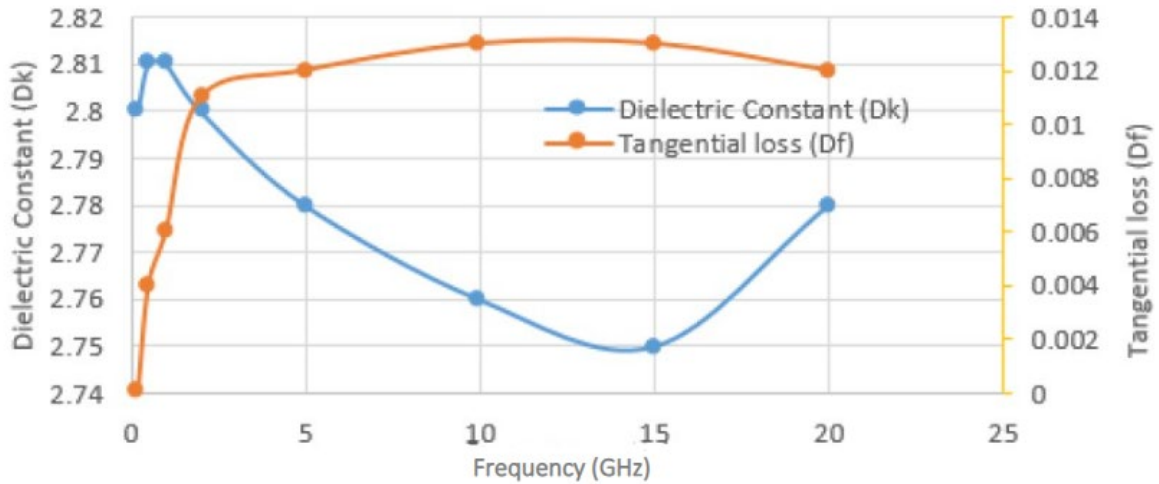


Figure 3: Dielectric properties of the acrylic ink [19].

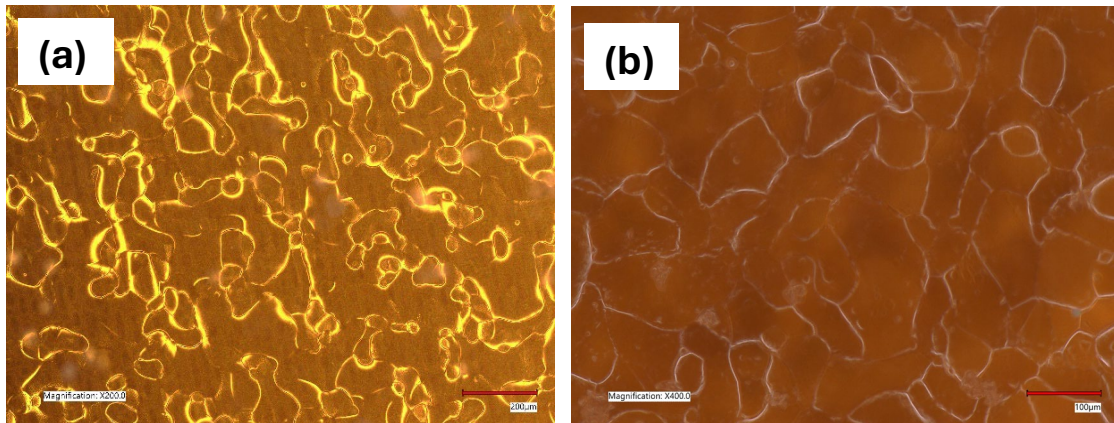


Figure 4: Morphology of the dielectric (Acrylic) ink after printing and curing.

A UV light cures the dielectric ink. As it contains a photo initiator, it is cured by photopolymerization. Optical microscopy was used to observe the surface morphology of the dielectric ink at various magnifications (Figure 4). It shows a uniform microstructure with no defects and pores.

**Resistors:**

Resistors were designed and fabricated using a Nano Dimension DragonFly IV system with conductive silver nanoparticle ink and acrylic polymer ink. A factorial design of experiments (DOE) was implemented to investigate the effects of resistor geometry, line width, layer thickness, and length on electrical resistance, as presented in Table 03. For each combination of parameters, multiple samples were printed. Theoretical resistance values were calculated based on designed geometries and known material properties. Experimental resistance values were measured using a source meter (Keithley 2450) at room temperature.

**Table 03:** Design of experiment for the single-layer resistors.

No. of resistor	Resistivity ( $\Omega/m$ )	Height, (m)	Width (m)	Area ( $mm^2$ )	Length, (m)	Theoretical Resistance ( $\Omega$ )
1	4.52E-08 ± 1.95E-08	3.00E-05	8.00E-05	2.4E-09	1.07E-02	0.201±0.086
2		3.00E-05	1.00E-04	3E-09	1.07E-02	0.161±0.069
3		4.50E-05	8.00E-05	3.6E-09	1.07E-02	0.134±0.058
4		4.50E-05	1.00E-04	4.5E-09	1.07E-02	0.107±0.046

The theoretical resistance was calculated according to the following equation:

$$R = \rho \frac{L}{A} \dots\dots\dots (3)$$

$$\text{Where, } \Delta R = \frac{\Delta \rho}{\rho} R \dots\dots\dots (4)$$

Contact resistance was 0.256 Ohms; this value was considered during the experimental resistance test.

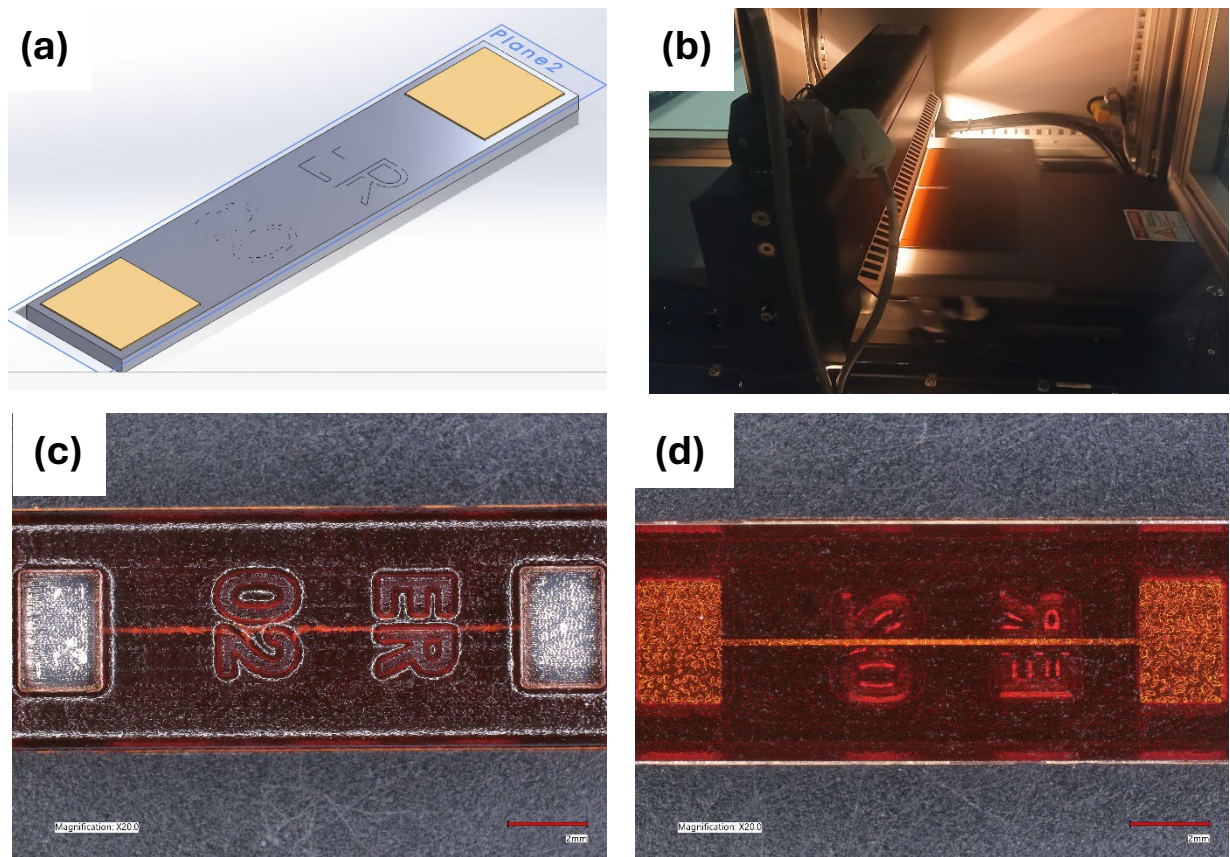


**Figure 5:** Fabrication process of single-layer embedded resistors (a) Design of the resistors using a 3D design software (SolidWorks) (b) printing using a 3D printer (DragonFly IV) (c) Front view of the printed resistor (d) Rear view of the resistor.

The fabricated samples exhibited a rigid structure, with the conductive pathways fully embedded within the dielectric material, as illustrated in Figure 5. This design offers a significant advantage in terms of environmental stability, as the encapsulation of the conductive elements effectively mitigates the risk of oxidation, which is an issue commonly encountered in conventionally additively manufactured resistors where the conductive traces are exposed on the surface. Oxidation of surface-exposed conductors typically leads to variations in resistance over time, thereby compromising the long-term reliability and performance consistency of such components. In contrast, the embedded architecture of our printed resistors ensures that their electrical properties remain stable, with no observable aging effects over extended periods. Furthermore, the resistors have excellent thermal stability, maintaining consistent performance at elevated temperatures up to 160 °C. We observed an excellent dimensional accuracy (Figure 6).

This robust performance profile highlights the suitability of the proposed fabrication approach for applications requiring reliable, long-lasting electronic components under demanding environmental conditions.

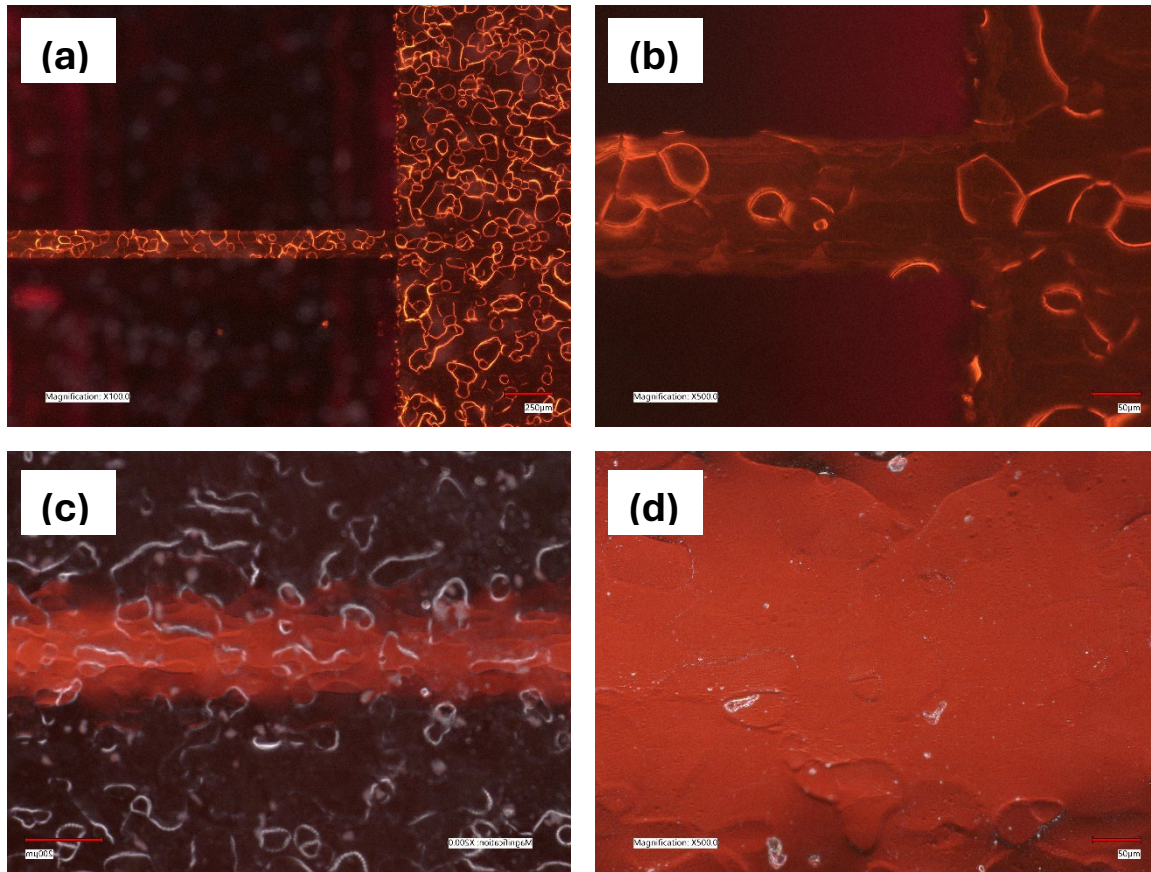


*Figure 6: Optical microscopic images of the printed resistors.*

**Table 04:** Resistance of the printed samples.

<b>Theoretical value, <math>R_{th}(\Omega)</math></b>	<b>Measured value <math>R_{ex}(\Omega)</math></b>	<b>Contact resistance <math>(\Omega)</math></b>	<b>Actual resistance <math>(\Omega)</math></b>
$0.201 \pm 0.086$	0.435	0.256	0.183
$0.161 \pm 0.069$	0.404		0.15
$0.134 \pm 0.057$	0.372		0.119
$0.107 \pm 0.049$	0.347		0.095

The resistance of the printed samples was measured by a source meter at room temperature. Our experimental values matched the theoretical values well with a small deviation. By adjusting the conductivity of printed silver ink, we can produce predictable resistor values. The length of the silver trace was the same for all four resistors. The area was varied to print the different resistors. The path length was small, which demonstrates that we can print embedded resistors inside the circuit.

**Multilayered resistor:**

As our ink is highly conductive, the resistance of our printed resistor was small. We have printed multilayered resistors to increase the resistance value. By creating the 3D structure, the length of the conductive path increased approximately 200 times. As a result, the resistance also increased.

**Table 05:** Design of experiment for the 3D resistor.

No. of resistor	Resistivity $\rho$ ( $\Omega/m$ )	Height, (m)	Width (m)	Area ( $m^2$ )	No. of layers	Length, (m)	Theoretical Resistance, ( $\Omega$ )
1	$4.52E-08$ $\pm$	$3.00E-05$	$2.00E-04$	$6.00E-09$	5	2.07	$15.60 \pm 6.72$
2	$1.95E-08$	$3.00E-05$	$8.00E-05$	$2.40E-09$	5	2.07	$38.99 \pm 16.81$

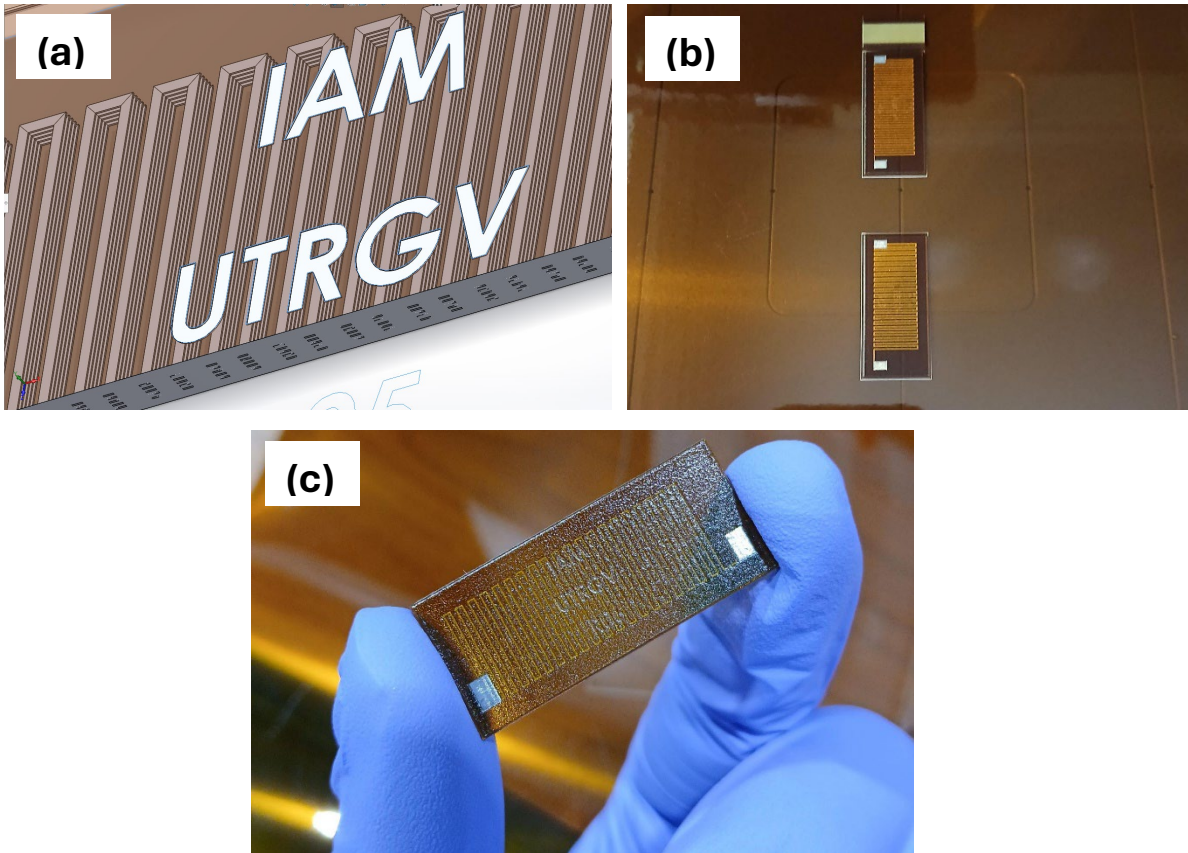


**Figure 7:** Fabrication process of the multilayered resistor (a) 3D design of the resistor (b), and (c) printed samples.

**Table 06:** Calculated value vs Experimental value.

Theoretical value, $R_{th}(\Omega)$	Measured value $R_{ex}(\Omega)$	Contact resistance( $\Omega$ )	Actual resistance ( $\Omega$ )
15.613±6.727	12.520	0.256	12.256
38.996±16.814	32.102		31.846

Figure 7 illustrates the 3D design of the printed resistors. The objective was to increase the resistance without enlarging the physical size of the resistor to achieve a compact design. We successfully fabricated multilayer resistors, and the measured resistance values aligned well with the expected results. The resistance increased by approximately 160 times compared to a single-layer resistor. This demonstrates that the resistance value can be effectively tuned by modifying the geometric structure of the resistor.

### Capacitor:

Capacitors are one of the fundamental passive components in electronic circuits, essential for energy storage, filtering, and signal coupling/decoupling. In this work, we successfully fabricated compact, multilayer functional capacitors using the DragonFly IV additive manufacturing system. The capacitors were printed in a fully integrated process, with 22 alternating layers of conductive silver nanoparticle ink and acrylic-based dielectric polymer. This multilayer architecture enabled a significant increase in capacitance density while maintaining a small overall footprint. The printed capacitors demonstrated stable electrical performance, with measured capacitance values in the nanofarad (nF) range, closely matching theoretical predictions based on layer geometry and material properties. These results underscore the potential of additive manufacturing for creating highly integrated, space-efficient passive components suitable for advanced electronic applications.

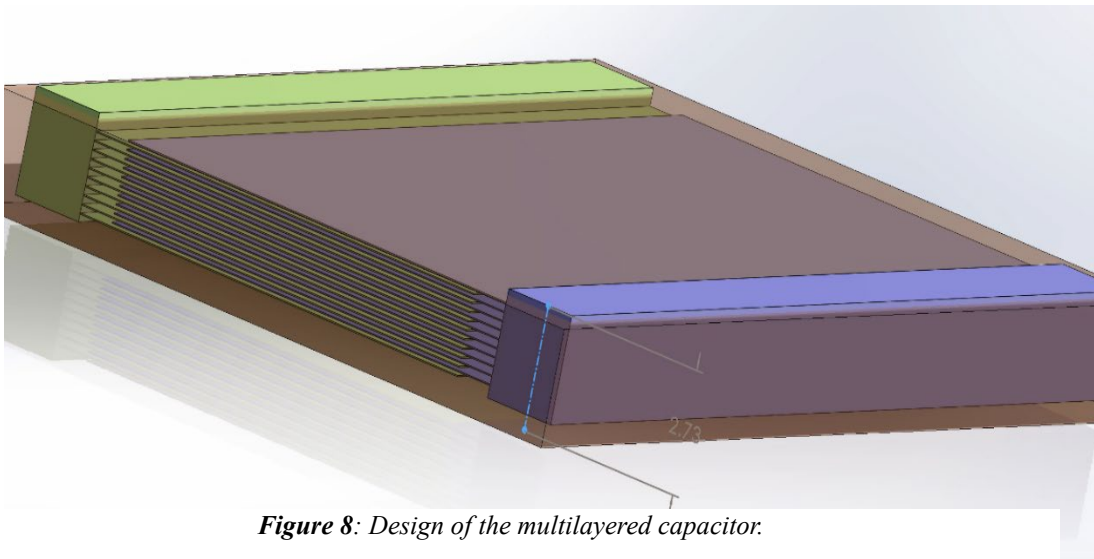


**Figure 8:** Design of the multilayered capacitor.

**Table 07:** Design of the experiment for the capacitor.

No. of capacitor	Relative permittivity $\epsilon_r$	Height (mm)	Width (mm)	Area (mm <sup>2</sup> )	Plate distance ( $\mu\text{m}$ )	No. of layers	Capacitance (nF)
1	2.96	10	15	150	70	22	1.18
2		10	25	250	70	22	1.97
3		20	15	300	70	22	2.36

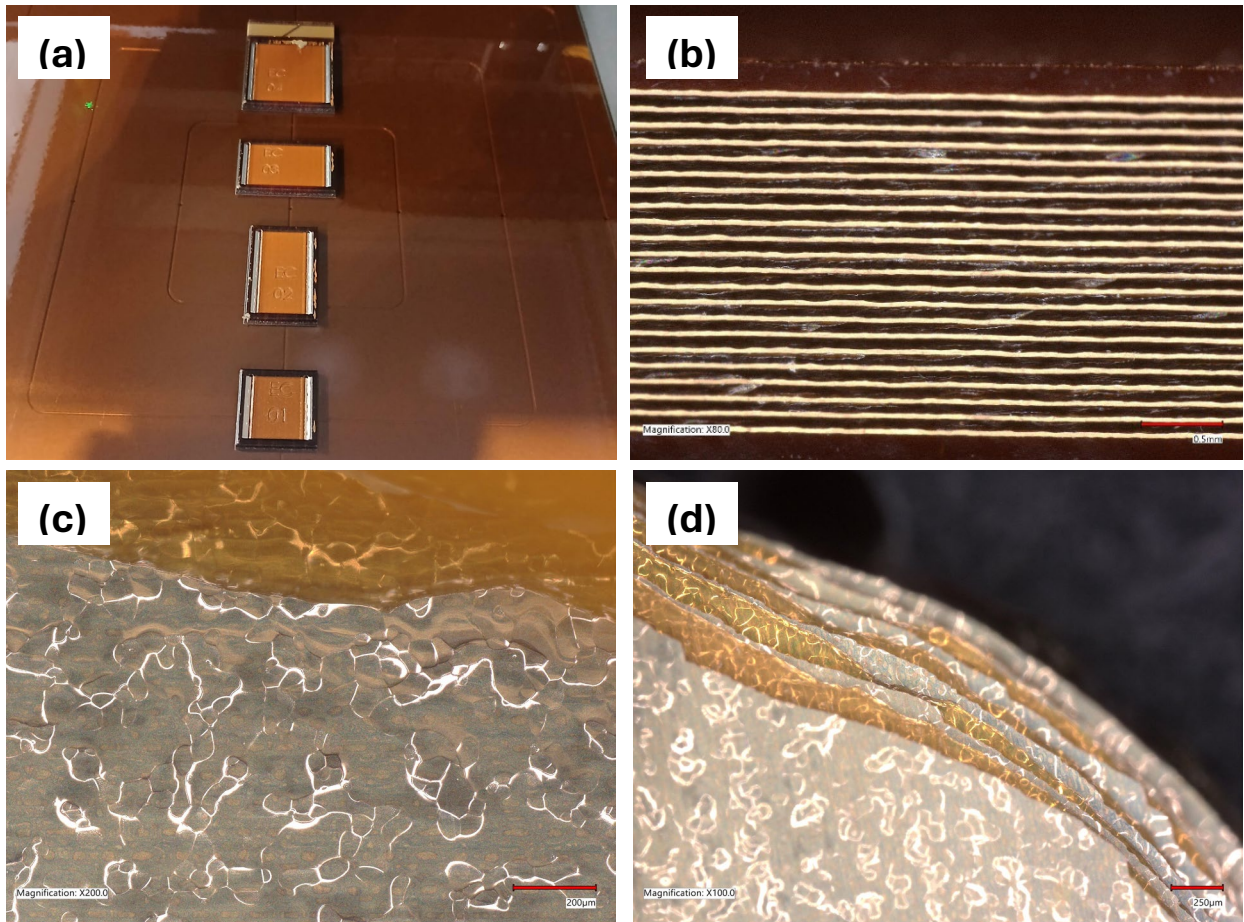


**Figure 9:** Morphology of the printed capacitor (a) After printing (b) Cross section of the capacitor (c) conductive layer (d) conductive and dielectric layer.

Figure 9 presents a detailed view of the conductive and dielectric layers within the printed structure. The spacing between adjacent conductive layers was measured to be approximately 70 microns, a dimension notably smaller than the diameter of a typical human hair. The multilayer architecture comprised 22 distinct conductive layers, all integrated within a total thickness of just 2 mm, demonstrating an exceptionally compact design. Moreover, conductive ink exhibited excellent curing characteristics, ensuring the formation of high-quality, defect-free conductive plates throughout the structure. This precise layer alignment and effective curing process contribute to the overall electrical integrity and mechanical stability of the printed component, making it highly suitable for advanced electronic applications requiring miniaturization and reliability.

The capacitance was calculated according to the following equation:

$$C = \frac{\epsilon A}{d} \dots\dots\dots (5)$$

Where, permittivity  $\epsilon = \epsilon_r \epsilon_0$ ,  $\epsilon_r$  = relative permittivity  $\epsilon_0$  = permittivity of free space (vacuum), with a value of approximately  $8.854 \times 10^{-12}$  F/m, and A= Area of the plate, d= distance between the plates.

Finally, the capacitance of the printed sample was measured by a multimeter.

**Table 08:** Experimental value vs theoretical value.

No. of Capacitors	Theoretical capacitance (nF)	Measured capacitance (nF)
1	1.18	1.52
2	1.97	2.52
3	2.36	2.98

The measured capacitance is slightly higher than the theoretical value, which may be attributed to variations in the dielectric thickness and increased effective permittivity of the printed layer. From the optical microscope images, we observe that the surface of the conductive layer is not smooth, which can increase the effective surface area of the plate as well. Overall, our printed capacitor is compact, and the value is satisfactory.

**RC Low-Pass Filter:**

Building on the successful fabrication of multilayer capacitors and resistors, we further integrated a compact RC low-pass filter (Figure 10) using the DragonFly IV additive manufacturing system. An embedded low-pass filter is crucial in RF applications, as it possesses lower parasitic capacitance.



*Figure 10: Printed low-pass RC filter.*

**Table 09:** Experimental values of the printed filter.

No. of filter	Resistance ( $\Omega$ )	Capacitance (nF)	Cut-off frequency (MHz)
1	11.63	6.95	1.97
2	46.58	7.02	0.49

The fully printed RC filter demonstrated stable and reproducible performance, underscoring the potential of additive manufacturing for integrating functional analog signal-processing circuits directly into compact, space-efficient electronic systems.

### **Analysis of RMS and Amplitude Ratios in the RC Low-Pass Filter**

Out of the two printed filters we made, one didn't survive the soldering step. The 3d printed connector plate was thin, and under the heat of the soldering iron, it melted away. This experience showed us that connector thickness is critical, and future designs should consider sturdier plates or gentler joining methods to avoid the same issue.

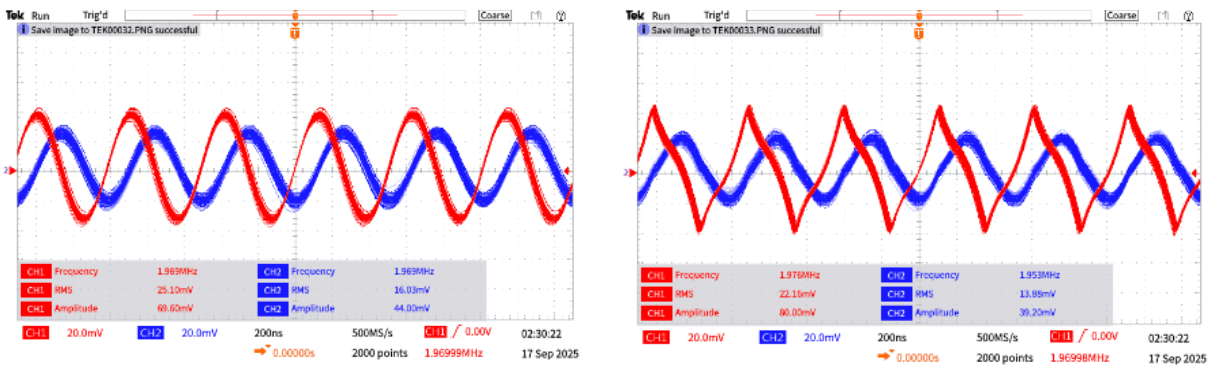
The RC low-pass filter was constructed with a 11.63  $\Omega$  resistor and a 6.95 nF capacitor in series. The input signal was applied across the entire RC branch, while the output was measured only across the capacitor, making it a standard first-order low-pass configuration. The theoretical cutoff frequency ( $f_c$ ) was about 1.97 MHz based on the following equation:

$$f_c = \frac{1}{2\pi RC} \dots \dots \dots (6)$$

where,  $f_c$  (Cutoff Frequency) is the frequency at which the filter begins to reduce the amplitude of the input signal significantly. At this point, the output drops to about 70% of the input amplitude (-3 dB). It marks the transition between frequencies that pass easily and those that are attenuated.  $R$  (Resistance) is the resistor value, measured in ohms ( $\Omega$ ), and  $C$  (Capacitance) is the capacitor value, measured in farads (F).

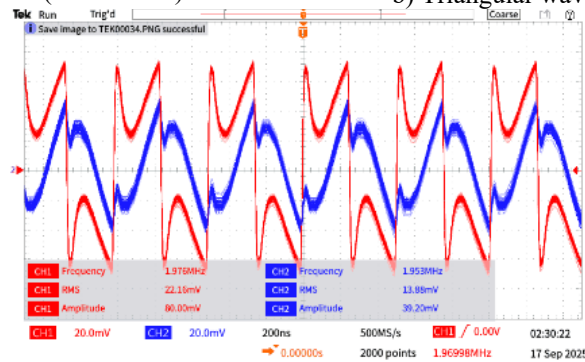
Figure 11(a-c) shows what happens to the sine, triangular, and square waves when the filter is driven right around its cutoff ( $\sim 1.97$  MHz). The sine wave just shrinks in size but keeps its shape, the triangular wave starts to smooth out, and the square wave distorts the most as its harmonics get cut away. These snapshots give a clear, time-domain picture of the filter's action before we look at the ratio plots in Figure 12 (a and b).

To study how it behaves, both the RMS ratio (output RMS/input RMS - Figure 12 a) and the amplitude ratio (output peak/input peak - Figure 12 b) were measured across different input frequencies and waveforms (sine, square, and triangular). A look at both ratios together allows us to see not only how much of the main signal passes through, but also how much of the harmonic content is affected.



(a) Sine wave at cutoff ( $\sim 1.97$  MHz).

(b) Triangular wave at cutoff ( $\sim 1.97$  MHz)



(c) Square wave at cutoff ( $\sim 1.97$  MHz).

**Figure 11:** RC filters output characteristics when subjected to (a) sine, (b) triangular, and (c) square waves.

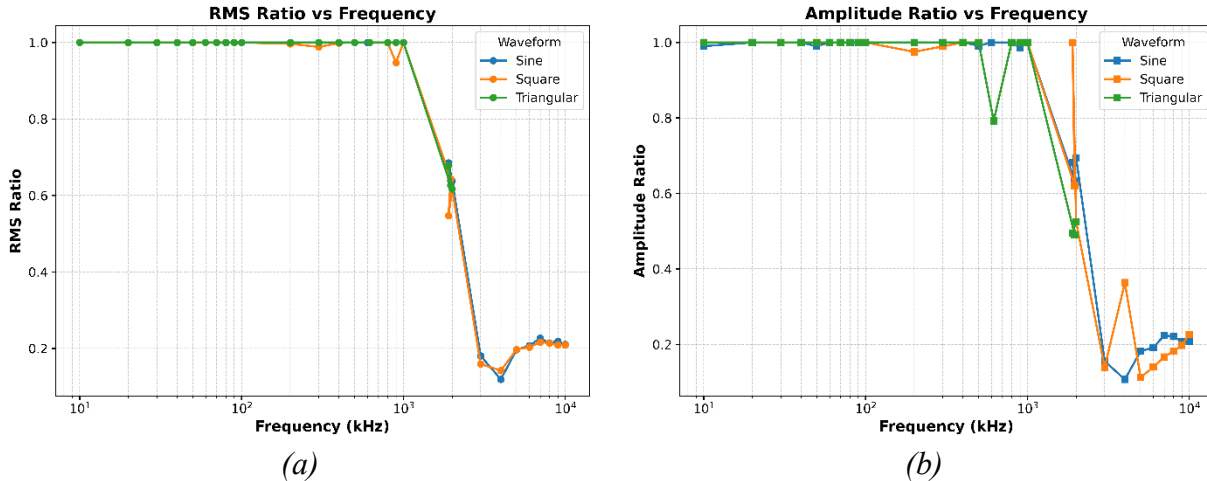


*Figure 12: (a) RMS ratio vs frequency, and (b) amplitude ratio vs frequency for sine, square, and triangular waveforms in the RC low-pass filter.*

At low frequencies, well below 2 MHz, the filter behaves as expected: the output closely matches the input, with both RMS and amplitude ratios remaining near unity. In this region, all three waveforms pass through with almost no distortion. As the frequency approaches the cutoff, however, the signal starts to weaken. For sine waves, this drop is smooth and follows the classic response of a first-order RC filter. Square and triangular waves show a faster fall in RMS ratio than in amplitude ratio, because their harmonics — especially the strong odd harmonics of the square wave — lie above the cutoff and are removed more aggressively. For instance, at 5 MHz the sine wave has an RMS ratio of about 0.20, and the square wave is nearly the same. However, the square wave’s amplitude ratio falls off more sharply, showing how the loss of harmonics has a stronger effect on non-sinusoidal signals. This explains why the output square wave appears more rounded and the triangular wave gradually loses its sharpness.

At frequencies well above the cutoff (beyond about 5 MHz), the filter is deep into its stopband. Here, both amplitude and RMS ratios drop below 0.2, showing strong attenuation of the signal. Sine waves fade predictably, while square and triangular waves are heavily smoothed. Square waves in particular lose almost all of their harmonic content, leaving only a sine-like trace at the output. Triangular waves, which already contain weaker harmonics, are less affected but still noticeably rounded.

Overall, the measured results line up well with the calculated cutoff of 1.97 MHz. Around this point, the amplitude ratio for sine waves falls to about 0.7, exactly what is expected at the  $-3$  dB frequency. The sharper RMS drop in non-sinusoidal inputs highlights how the filter not only reduces signal strength but also reshapes waveforms by cutting away their harmonics. Since the dataset covers a wide frequency range—from 10 kHz up to 10 MHz, nearly three decades—the agreement with theory is very clear. It captures all the key regions: the flat passband at low frequencies, the transition around cutoff, and the strong attenuation in the stopband. As expected for a first-order RC circuit, the roll-off beyond cutoff is close to  $-20$  dB per decade.

## **Conclusions**

We have successfully fabricated various fundamental passive electronic components, such as resistors and capacitors, using PCB printing technology. The printed resistors are embedded within the board, making them resistant to corrosion and oxidation. We also printed multilayered resistors with complex geometries, which resulted in increased resistance values. The resistance of single-layer resistors was measured at less than 1  $\Omega$ , while multilayered resistors of the same size achieved a resistance of 31.8  $\Omega$ . These resistance values closely matched our design targets, demonstrating that we can accurately print resistors with specific resistance values embedded directly into the circuit. Furthermore, the resistance can be adjusted by modifying the geometry of the resistor without compromising the sizes of the components. This method enables the production of very small and compact components within the circuit. We have also fabricated multilayer compact capacitors using the same printing technology. The capacitance of these capacitors is in the nano-farad range, which results in cutoff frequencies in the megahertz (MHz) range. This suggests that they are suitable for use in radio frequency (RF) applications. Since the relative permeability of the dielectric ink is approximately 1, the capacitors do not suffer from magnetic losses. Additionally, by embedding these capacitors directly into the circuit board, it is possible to eliminate the need for soldering external capacitors, leading to more compact and reliable designs.

Compared to earlier studies on printed passive components, our work brings three key advantages: (i) the components are embedded directly into the substrate, making the design more compact, (ii) the conductive pathways are protected from oxidation, which improves long-term reliability, and (iii) the performance can be predictably tuned by geometry, without the need for extra post-processing. At the same time, there's still plenty of room for improvement. For example, the dielectric material limits how much capacitance we can achieve, and the performance of our components at frequencies beyond the MHz range still needs to be tested. In future work, we plan to extend this approach to include inductors and full RLC networks, which could lead to fully integrated printed filters and power circuits. Overall, this study shows that additive manufacturing of embedded passives is not just possible, but also practical for creating smaller, more durable, and customizable circuits. These advances could make a real difference in applications ranging from space-constrained wearable IoT devices to aerospace electronics that need to remain reliable under extreme conditions.

## **Acknowledgements**

The authors would like to acknowledge funding provided by the U.S. Department of Defense under Award No. W911NF-25-2-0030. The opinions expressed in this paper are solely those of the authors and do not necessarily represent those of the U.S. Department of Defense.

## References

- [1] A. E. Ostfeld, I. Deckman, A. M. Gaikwad, C. M. Lochner, and A. C. Arias, "Screen printed passive components for flexible power electronics," *Sci. Rep.*, vol. 5, no. 1, p. 15959, Oct. 2015, doi: 10.1038/srep15959.
- [2] S. Jung, A. Sou, E. Gili, and H. Sirringhaus, "Inkjet-printed resistors with a wide resistance range for printed read-only memory applications," *Org. Electron.*, vol. 14, no. 3, pp. 699–702, Mar. 2013, doi: 10.1016/j.orgel.2012.12.034.
- [3] H. A. Hobbie, J. L. Doherty, B. N. Smith, P. Maccarini, and A. D. Franklin, "Conformal printed electronics on flexible substrates and inflatable catheters using lathe-based aerosol jet printing," *Npj Flex. Electron.*, vol. 8, no. 1, p. 54, Aug. 2024, doi: 10.1038/s41528-024-00340-0.
- [4] C. Zhang *et al.*, "Additive-free MXene inks and direct printing of micro-supercapacitors," *Nat. Commun.*, vol. 10, no. 1, p. 1795, Apr. 2019, doi: 10.1038/s41467-019-09398-1.
- [5] I. Piekarz, K. Wincza, S. Gruszczynski, and J. Sorocki, "Low-cost fully additively manufactured passive microwave components exploiting available 3D flexibility," *Sci. Rep.*, vol. 13, no. 1, p. 2886, Feb. 2023, doi: 10.1038/s41598-023-30163-4.
- [6] T. Reinheimer, V. Baumann, and J. R. Binder, "Fabrication of Flexible Multilayer Composite Capacitors Using Inkjet Printing," *Nanomaterials*, vol. 10, no. 11, p. 2302, Nov. 2020, doi: 10.3390/nano10112302.
- [7] M. Mikolajek, T. Reinheimer, N. Bohn, C. Kohler, M. J. Hoffmann, and J. R. Binder, "Fabrication and Characterization of Fully Inkjet Printed Capacitors Based on Ceramic/Polymer Composite Dielectrics on Flexible Substrates," *Sci. Rep.*, vol. 9, no. 1, p. 13324, Sep. 2019, doi: 10.1038/s41598-019-49639-3.
- [8] H. W. Tan, T. Tran, and C. K. Chua, "A review of printed passive electronic components through fully additive manufacturing methods," *Virtual Phys. Prototyp.*, vol. 11, no. 4, pp. 271–288, Oct. 2016, doi: 10.1080/17452759.2016.1217586.
- [9] G. McKerricher, J. Gonzalez Perez, and A. Shamim, "Fully Inkjet Printed RF Inductors and Capacitors Using Polymer Dielectric and Silver Conductive Ink With Through Vias," *IEEE Trans. Electron Devices*, vol. 62, no. 3, pp. 1002–1009, Mar. 2015, doi: 10.1109/TED.2015.2396004.
- [10] S.-Y. Wu, C. Yang, W. Hsu, and L. Lin, "3D-printed microelectronics for integrated circuitry and passive wireless sensors," *Microsyst. Nanoeng.*, vol. 1, no. 1, p. 15013, Jul. 2015, doi: 10.1038/micronano.2015.13.
- [11] X. Peng *et al.*, "Integrating digital light processing with direct ink writing for hybrid 3D printing of functional structures and devices," *Addit. Manuf.*, vol. 40, p. 101911, Apr. 2021, doi: 10.1016/j.addma.2021.101911.
- [12] V. K. S. Yadav, G. Natu, and R. P. Paily, "Fabrication and Electrical Characterization of Printed Microresistors of Silver Nanoparticles Using Microcantilever-Based Printing Technology," *IEEE Trans. Compon. Packag. Manuf. Technol.*, vol. 10, no. 1, pp. 57–64, Jan. 2020, doi: 10.1109/TCPMT.2019.2954079.
- [13] C. Tomassoni, O. A. Peverini, G. Venanzoni, G. Addamo, F. Paonessa, and G. Virone, "3D Printing of Microwave and Millimeter-Wave Filters: Additive Manufacturing Technologies Applied in the Development of High-Performance Filters with Novel Topologies," *IEEE Microw. Mag.*, vol. 21, no. 6, pp. 24–45, Jun. 2020, doi: 10.1109/MMM.2020.2979153.
- [14] K. M. K. H. Leong, E. Nguyen, J. Tice, and V. Radisic, "3D Printed Folded Monopole Antennas," in *2023 IEEE International Symposium on Antennas and Propagation and*

- USNC-URSI Radio Science Meeting (USNC-URSI)*, Portland, OR, USA: IEEE, Jul. 2023, pp. 1081–1082. doi: 10.1109/USNC-URSI52151.2023.10238205.
- [15] U. Robles, E. Bustamante, P. Darshni, and R. C. Rumpf, “HIGH-FREQUENCY FILTERS MANUFACTURED USING HYBRID 3D PRINTING METHOD,” *Prog. Electromagn. Res. M*, vol. 84, pp. 147–155, 2019, doi: 10.2528/PIERM18102603.
- [16] Y. Niu *et al.*, “Synthesized silver nanoparticles decorated reduced graphene oxide/silver ink for aerosol jet printed conformal temperature sensor with a wide sensing range and excellent stability,” *J. Mater. Res. Technol.*, vol. 25, pp. 873–886, Jul. 2023, doi: 10.1016/j.jmrt.2023.05.246.
- [17] H. Yuk *et al.*, “3D printing of conducting polymers,” *Nat. Commun.*, vol. 11, no. 1, p. 1604, Mar. 2020, doi: 10.1038/s41467-020-15316-7.
- [18] N. Ibrahim, J. O. Akindoyo, and M. Mariatti, “Recent development in silver-based ink for flexible electronics,” *J. Sci. Adv. Mater. Devices*, vol. 7, no. 1, p. 100395, Mar. 2022, doi: 10.1016/j.jsamd.2021.09.002.
- [19] Nano Dimension, “DragonFly IV Product.” <https://www.nano-di.com/dragonfly-iv>